Oceanic mega-impacts and crustal evolution

Andrew Y. Glikson
Research School of Earth Science, Australian National University, Canberra, A.C.T. 0200, Australia

ABSTRACT

Lunar mare crater counts, the terrestrial impact flux, and astronomical observations of asteroids and comets define a consistent impact rate of 4–6 • 10^{-15} km^{-2} • yr^{-1} within the inner solar system since the end of the late heavy bombardment ~3.8 Ga. Coupled with the observed crater size vs. cumulative crater size frequency relationship of $N \propto D_c^{-1.8}$ (N = cumulative number of craters of diameter >D_c), these rates imply formation on Earth of more than 450 D_c ≥100-km-diameter craters, more than 50 D_c ≥300-km-diameter craters, and more than 20 D_c ≥500-km-diameter craters. Geochemical and isotopic constraints require that more than 80% of the projectiles impacted on time-integrated oceanic crust since the late heavy bombardment. The injection of shock energies calculated at >10^8 Mt TNT equivalent by a D_p >10-km-diameter projectile may result in propagating fractures and rift networks, thermal perturbations, and ensuing magmatic activity. Examinations of the geologic record for correlated impact and magmatic fingerprints of such events remain inconclusive in view of isotopic age uncertainties. Potential but unproven connections may be represented by the (1) Cretaceous-Tertiary boundary (ca. 65 Ma) impact(s), onset of the Carlsberg Ridge spreading, Deccan volcanism, and onset of the mantle plume of the Emperor-Hawaii chain; (2) Jurassic-Cretaceous boundary (ca. 145 Ma) impacts, onset of Gondwana breakup, including precursors of the East African rift structures; (3) Permian-Triassic boundary (ca. 251 Ma) impact(s), Siberian Norilsk traps, and Early Triassic rifting; and (4) the 3.26 Ga basal Fig Tree Group (east Transvaal) Ir-rich and Ni-rich quench spinel-bearing impact spherules and contemporaneous igneous-tectonic activity. Tests of the theory require further identification and isotopic dating of distal ejecta, impact spherule condensates, and meteoritic geochemical anomalies.

OBSERVED AND PREDICTED MEGA-IMPACT RATES

It is widely accepted that meteoritic impacts constituted the single most important factor in shaping the surfaces of the terrestrial planets during the late heavy bombardment ca. 4.2–3.8 Ga, when the estimated flux for craters having diameters (D_c) ≥18 km was 4–9 • 10^{-13} km^{-2} • yr^{-1} (Baldwin, 1985; Ryder, 1990). Post-bombardment lunar and terrestrial crater counts yield consistent impact rates within the range of 3.8–6.3 • 10^{-15} km^{-2} • yr^{-1}, consistent with the cratering rate of 5.9 ± 3.5 • 10^{-15} km^{-2} • yr^{-1} estimated for near-Earth asteroids and comets (Shoemaker and Shoemaker, 1996).

Lunar and terrestrial crater counts indicate crater size vs. cumulative size frequency relationships approximating $N \propto D_c^{-1.8}$ to $N \propto D_c^{-2.0}$ (D_c = crater diameter; N = cumulative number of craters with diameters >D_c). By projecting cratering rates for craters of D_c ≥20 km to the entire Earth surface, and assuming post–late heavy bombardment lunar crater size vs. crater size frequency relationships of $N \propto D_c^{-1.8}$ (Shoemaker and Shoemaker, 1996), estimates can be made of the number of terrestrial craters formed since ca. 3.8 Ga (Fig. 1; Table 1). Because of a probable uneven size distribution of asteroids and comets, in particular in the larger size categories, cumulative crater size vs. size frequency plots represent mean rather than originally linear relationships. The terrestrial record of impact by projectiles

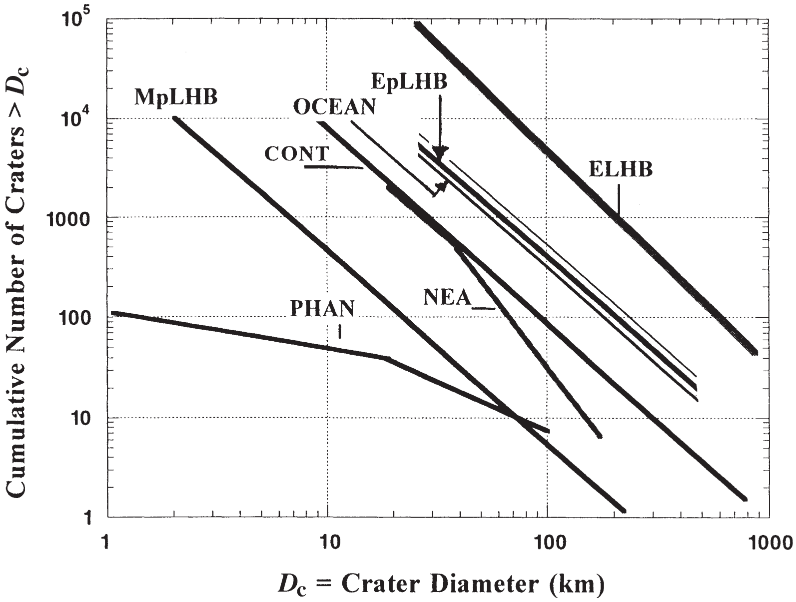

Figure 1. Crater size vs. cumulative frequency plots for post–late heavy bombardment time in Earth-Moon system. MpLHB—post-lunar maria craters and post-Martian plains craters (after Barlow, 1990). NEA—crater distribution extrapolated from observed near earth asteroids (D_c = 20 D_p [p is projectile]). PHAN—Phanerozoic impact rates after Grieve and Dence (1979), showing loss of smaller craters. EpLHB—average Earth cratering rate based on Table 1 and extrapolated to entire Earth surface on basis of number of ≥20-km-diameter craters and cumulative crater vs. size-frequency relationships parallel to those of MpLHB. CONT—mean cratering rate on time-integrated continental crust (~20% of Earth's surface). OCEAN—mean cratering rate on time-integrated ocean crust (~80% of Earth's surface). ELHB—late heavy bombardment of Earth, extrapolated from lunar data of Barlow (1990).

TABLE 1. ESTIMATES OF POST–3.8 GA TERRESTRIAL IMPACT RATES

	Refs.*	Number of craters, D_c				
		≥20 km	≥100 km	≥300 km	≥500 km	≥1000 km
Cratering rate ($R \cdot 10^{-15}$ km$^{-2} \cdot$ yr^{-1})						
4.3 ± 0.4	1	8300	390	45	17	4
3.8 ± 1.9	2	7350	320	36	14	3
6.3 ± 3.2	3	12 200	560	74	24	6
5.6 ± 2.8	4	10 840	470	56	20	5
5.9 ± 3.5	5	11 450	520	60	22	6
5.5 ± 2.7	6	10 630	460	54	19	5
Mean = 5.23		10 130	450	53	19	5
Predicted number of continental craters		2026	90	11	4	1
Predicted number of oceanic craters		8104	363	42	15	4
Number of observed continental craters		39	8	?3 with D_c ≥ 250	N.A.	N.A.
Observed/predicted craters (%)						
Entire Earth surface		0.38	1.8	<5	N.A.	N.A.
Continental crust†		1.9	8.9	<25	N.A.	N.A.

Note: Based on literature estimates for craters with D_c ≥20 km, and on projected crater numbers for craters with D_c ≥100 km, ≥300 km, ≥500 km, and ≥1000 km, projected from crater size vs. cumulative crater size plots with $N \propto D_c^{-1.8}$. Numbers of craters are rounded. The number of craters with D ≥250 km assumes Morokweng to be a crater ~ 340 km in diameter (Corner et al., 1997) and Sudbury as a 200–250-km-diameter crater (Deutsch, 1998).

*References: 1—Terrestrial cratering rate equivalent to the lunar cratering rate ~3.2 Ga; asteroid impact velocities assumed (Shoemaker and Shoemaker, 1996); 2—Proterozoic impact rate estimated from Australian impact structures (Shoemaker and Shoemaker, 1996); 3—Phanerozoic impact rates estimated by extrapolation from impact structures D_c ≥10 km in central United States (Shoemaker and Shoemaker, 1996); 4—Cratering rate since 120 Ma (Grieve and Shoemaker, 1994); 5—Present cratering rate estimated from astronomical surveys (Shoemaker and Shoemaker, 1996); 6—Terrestrial cratering rate for craters of D_c ≥ 20 km (Grieve and Pesonen, 1996)

†Time-integrated continental crust area.

with D_p >10 km is confirmed by structures such as the Vredefort ring (~300 km; Deutsch, 1998), possibly the Morokweng structure (~340 km; Corner et al., 1997, but possibly only 70 km diameter; Hart et al., 1997), and the Sudbury basin (200–250 km; Deutsch, 1998). Several suggested impact structures remain unconfirmed, including large circular structures in Fennoscandia (Nunjes, D ~400 km; Uppland, D ~300 km; Marras, D ~250 km) (Pesonen, 1996), and several Australian structures (Gorter, 1998). Estimates of post–late heavy bombardment craters with D_c ≥500 km are supported by astronomical observation of corresponding near-Earth asteroids, e.g., Swift Tuttle (D_p = 24 km).

OCEANIC IMPACT RATES

Preservation of the terrestrial impact record is hampered by uplift, erosion, burial, and metamorphism of continental crust and, most important, subduction of pre–200 Ma oceanic crust. Thus, the terrestrial impact record is strongly skewed in favor of young and large impact structures (Fig. 1). The terrestrial impact record of 156 craters observed to date (R. A. F. Grieve, 1997, personal commun.) includes 67 structures with D_c ≥10 km and 39 with D_c ≥20 km. The terrestrial cratering data suggest positive relationships between crater size and degree of preservation. Thus, the up-to-date observed terrestrial record of 39 craters with D_c ≥20 km forms ~0.39% of the predicted number (~10 130), the eight observed craters with D_c ≥100 km form 1.8% of the predicted flux, and the possible three observed craters with D_c ≥250 km form ~5% of the predicted flux (Table 1).

Geochemical and isotopic estimates of growth rates of sialic crust (McCulloch and Bennett, 1994) suggest that the time-integrated area occupied by oceanic crust since the late heavy bombardment constituted >80% of Earth's surface. Assuming three continental impact structures with D_c ≥250, a minimum of 12 oceanic craters of this size range is implied, compared to a predicted number of ~42 oceanic craters (Table 1). However, with the exception of Mjolnir (D_c = 40 km; 143 ± 20 Ma; R. A. F. Grieve, 1997, personal commun.) and Eltanin (Gersonde et al., 1997), no oceanic impact structures have been observed to date, due to current-induced burial and possibly inundation of large craters by volcanic flows. Pre–200 Ma oceanic impact structures would have been eliminated by subduction.

More than 10% of present-day oceanic crust is spatially associated with sea-floor spreading centers overlying shallow asthenosphere where geothermal gradients may be more than 20 °C/km. Higher heat-flow values and geothermal gradients are estimated for Precambrian oceanic regimes and have been modeled in terms of small-scale convection cells and crustal plates as compared to modern oceanic regimes (Green, 1981). The extent of Precambrian oceanic crust that was thin (<5 km depth to Moho) and overlay shallow (~30–40 km) asthenosphere may have therefore been >20% of the ocean basins. From impact rate and size distribution estimates (Table 1), more than 70 craters with D_c ≥100 and more than eight craters with D_c ≥300 km would have formed in near-ridge ocean crust in post–late heavy bombardment time (Table 1).

CONSEQUENCES OF LARGE OCEANIC IMPACTS

Model predictions of the consequences of large oceanic impacts (Jansa, 1993) and computer simulations (Roddy et al., 1987) suggest that the water column had negligible effects, and cratering effects were on a scale similar to continental impacts. The formation of a 100-km-diameter crater can be modeled in terms of impact by a chondritic (3.0 g/cm^3) projectile (p) with D_p ~5 km and a typical approach velocity of 24.6 km/s^{-1} (Grieve, 1980). Penetration to a depth of 6–8 km (~1.5 D_p) and explosive energy (E) release on the scale of E ≥10^{22} J (>10^6 Mt TNT equivalent) result in a transient crater (tc) with D_{tc} ~50–60 km, followed by elastic rebound and expansion into a ring structure with a diameter of ~2 D_{tc} (~20 D_p). The crustal column affected by the rebound (structural uplift, U_s), observed as $U_s = 0.086\ D_c^{1.03}$ (Grieve and Pilkington, 1996), will be ~10 km, resulting in ~3.3 kbar decompression of underlying mantle. Computer modeling by Roddy et al. (1987) for impact by a D_p = 10 km asteroid indicates excavation of a transient oceanic crater with D_c = 105 km and a depth (d) of d_{tc} ~27 km, followed by rebound effects through a depth similar to or greater than d_{tc}. The extent of rebound-induced adiabatic melting in the mantle is related to the local geothermal gradient and to a lesser extent shock heating (Grieve, 1980) (Fig. 2). A lower limit on the volume of affected crust and lithosphere approximates a vertical cylinder defined by U_s and D_c. Impacts producing craters D_c = 100 km and D_c = 300 km will affect volumes of crust and lithosphere of about $9 \cdot 10^5$ km^3 and $2.2 \cdot 10^6$ km^3, respectively. For craters with D_c = 300 km and 10%–50% mantle melting, volumes of produced magma range from $0.22 \cdot 10^6$ km^3 for basaltic magmas to $1.1 \cdot 10^6$ km^3 for peridotitic komatiite magma.

It is relevant to compare the volumes of modeled impact-rebound–produced basalt relative to continental plateau basalts, oceanic large igneous provinces, and Archean mafic-ultramafic volcanism. Estimated volumes of continental basalts and their hypabyssal equivalents (Columbia Plateau: ~10^6 km^3; North Atlantic volcanic province: ~$7 \cdot 10^6$ km^3; Deccan traps: ~$8 \cdot 10^6$ km^3) (Coffin and Eldholm, 1994) and minimum volumes of Archean greenstones (ca. 3.47 Ga Warrawoona Group, Pilbara craton, Western Australia: >$0.25 \cdot 10^6$ km^3; ca. 2.7 Ga greenstones in the Eastern Goldfields, Western Australia: >$2 \cdot 10^6$ km^3), and the largest large igneous provinces (Ontong-Java Plateau: $3.6–5.5 \cdot 10^7$ km^3; Kerguelen Plateau: $1.6–2.4 \cdot 10^7$ km^3) are similar to, or larger by an order of magnitude than, modeled volumes of impact-produced basalts.

Large impact events on thin (<5 km), geothermally active (>25 °C km^{-1}) oceanic crust overlying shallow asthenosphere (<40 km) may result in localization and/or accentuation of mantle convection cells and sea-floor spreading centers. Green (1981) suggested that Archean peridotitic komatiites formed by ~50% catastrophic melting upon lithospheric rebound, ascent of mantle diapirs, adiabatic melting, and intersection of the hydrous and dry pyrolite solidi at upper asthenospheric levels (Fig. 2). At pressures of >60 kbar, smaller degrees of melting can produce ultrabasic melts (C. G. Ballhaus, 1998, personal commun.).

Under the high heat-flow levels prevailing in Archean oceanic regimes, the basaltic crust would not transform into eclogite, placing constraints on the density-driven subduction model (Green, 1981). An alternative model involving impact-triggered episodic two-stage mantle-melting processes (Glikson, 1993, 1996) includes: (1) large-scale melting of rebounding suboceanic asthenosphere; (2) gravitational collapse of thick slabs of oceanic crust dominated by high-density peridotite komatiite (>14% total iron as FeO; ~3.4 g/cm^3) into underlying olivine-dominated lower density asthenosphere (~3.3 g/cm^3); and (3) anatexis, production of dacitic melts, and accretion of sialic nuclei.

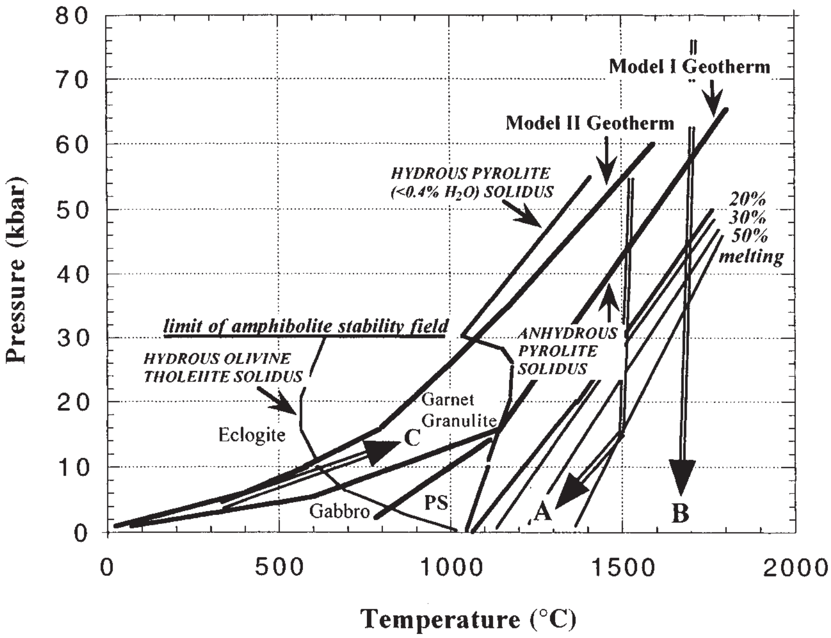

Figure 2. Pressure (*P*) vs. temperature (*T*) plot of oceanic geothermal regimes, metamorphic *P-T* fields, hydrous and anhydrous solidi of mantle and crust materials, and percent melting curves for anhydrous mantle (after Green, 1981). PS—superposed postshock heat effects (after Grieve, 1980). Boundaries show anhydrous pyrolite solidus, hydrous pyrolite solidus, amphibole breakdown curve, basalt melting curve, and hydrous basalt melting curve. Model geotherms: Model I—oceanic geotherm (~25 °C/km); model II—continental geotherm (~12 °C/km). Arrows: A—rebound *P-T* transport path of mantle excavated by 100-km-diameter crater with central uplift of 10 km; B—rebound *P-T* transport path of mantle excavated by 300-km-diameter crater with central uplift of 30 km; C—subsidence and partial melting *P-T* transport path of high-density komatiite-dominated mafic crust collapsed into olivine-dominated residual mantle.

POTENTIAL CORRELATIONS BETWEEN MEGA-IMPACTS AND CRUSTAL MAGMATIC AND TECTONIC EPISODES

Criteria for identification of proposed impact-triggered faults, rift structures, and distal igneous activity (Alt et al., 1988; Oberbeck et al., 1992; Jones, 1987, Hughs et al., 1977) remain undefined. The meager number of precisely dated impact events, contrasted with the extensive body of isotopic ages of magmatic events, results in a strongly skewed database that does not allow a statistically meaningful test of significant correlations. However, the terrestrial impact flux considered here, coupled with the episodic nature of major magmatic events (Moorbath, 1977; Condie, 1995; Glikson, 1993, 1996), may hint that these phenomena are interrelated. Pending further documentation of the terrestrial impact record (Table 2 in Glikson, 1996), potential targets for further testing include: (1) Jurassic-Cretaceous boundary impacts (ca. 145 Ma—Morokweng, Gosses Bluff, Mjolnir), breakup of the southern part of Gondwana, and initiation of the Mesozoic precursor of the Syrian-African rift system; (2) Cretaceous-Tertiary boundary impact(s) (65 Ma—Chicxulub) and the onset of Deccan volcanism (Alt et al., 1988), onset of Carlsberg Ridge spreading, and onset of the Emperor-Hawaii chain (64.7 Ma); (3) Late Triassic impacts (ca. 214 Ma—Manicouagan, Saint Martin, Puchezh-Katunki) and extensive rifting and alkalic volcanic activity; (4) the Araguainha impact, Brazil (ca. 244 Ma), a possible manifestation of a larger impact cluster, and the Siberian volcanic traps (248 ± 2.4 Ma); and (5) the basal Fig Tree Group impact spherules (ca. 3.26 Ga), east Transvaal, identified by iridium anomalies and unique Ni-rich quench spinels, inferred to be produced by a bolide ~40 km in diameter (Byerly and Lowe, 1994), and major contemporaneous igneous and tectonic activity in the Pilbara craton, Western Australia. Each of these correlations is subject to uncertainties arising from error margins of isotopic ages, e.g. the possible pre-Chicxulub age of the Deccan basalts (Alt et al., 1988).

Compilations of Precambrian isotopic data have been interpreted in terms of continuous crustal accretion, distinct thermal and tectonic episodes (Condie, 1995; Glikson, 1993, 1996), or combined episodicity and accretion (Card, 1990). The global nature of these episodes is suggested by correlations between peak periods of thermal events in separate Precambrian shields. However, the significance of age-distribution histograms is fraught with uncertainties arising from the likely selective preservation of crustal segments and from sampling bias due to economic and scientific priorities and terrain inaccessibility. The tentative episodic nature of mafic igneous activity suggested by age distribution diagrams may be interpreted in terms of purely endogenic factors (Davies, 1995), effects of mega-impacts (Glikson, 1993, 1996), or a combination of both. The role of large impacts in crustal evolution will be identified by their distal signatures—spherulitic melt condensates (microkrystites), microtektites, platinum-group-element anomalies, shocked quartz and zircon, distal ejecta, earthquake-generated rip-up clasts, and tsunami deposits. Pending these tests, as pointed out by Carl Sagan: “Absence of evidence is not evidence of absence.”

ACKNOWLEDGMENTS

I thank C. S. Shoemaker for comments on this manuscript, and J. W. Geissman and T. R. Watters for comments on an earlier version.

REFERENCES CITED

Alt, D., Sears, J. M., and Hyndman, D. W., 1988, Terrestrial maria: The origins of large basalt plateaus, hot spots tracks and spreading ridges: Journal of Geology, v. 96, p. 647–662.

Baldwin, R. B., 1985, Relative and absolute ages of individual craters and the rates of infalls on the Moon in the post-Imbrium period: Icarus, v. 61, p. 63–91.

Barlow, N. G., 1990, Estimating the terrestrial crater production rate during the late heavy bombardment period, *in* Abstracts for the International workshop on Meteorite impact on the early Earth: Lunar and Planetary Institute Contribution 746, p. 4–7.

Byerly, G. R., and Lowe, D. R., 1994, Spinels from Archean impact spherules: Geochimica et Cosmochimica Acta, v. 58, p. 3469–3486.

Card, K. D., 1990, A review of the Superior province of the Canadian Shield, a product of Archaean accretion: Precambrian Research, v. 48, p. 99–156.

Coffin, M. F., and Eldholm, O., 1994, Large igneous provinces: Crustal structure, dimensions and external consequences: Reviews of Geophysics, v. 32, p. 1–36.

Condie, K. C., 1995, Episodic ages of greenstone: A key to mantle dynamics?: Geophysical Research Letters, v. 22, p. 2215–2218.

Corner, B., Reimold, W. U., Brandt, D., and Koeberl, C., 1997, Morokweng impact structure, Northwest province, South Africa: Geophysical imaging and shock petrographic studies: Earth and Planetary Science Letters, v. 146, p. 351–364.

Davies, G. F., 1995, Punctuated crustal evolution of the Earth: Earth and Planetary Science Letters, v. 136, p. 363–379.

Deutsch, A., 1998, Examples for terrestrial impact structures, *in* Marfunin, A. S., ed., Advanced mineralogy, Volume 3: Berlin, Springer-Verlag, p. 119–129.

Gersonde, R., Kyte, F. T., Bleil, U., Diekmann, B., Flores, J. A., Gohl, K., Grahl, G., Hagen, R., Kuhn, G., Sierro, F. J., Volker, D., Abelmann, A., and Bostwick, J. A., 1997, Geological record and reconstruction of the late Pliocene impact of the Eltanin asteroid in the Southern Ocean: Nature, v. 390, p. 357–363.

Glikson, A. Y., 1993, Asteroids and early Precambrian crustal evolution: Earth-Science Reviews, v. 35, p. 285–319.

Glikson, A. Y., 1996, Mega-impacts and mantle melting episodes: Tests of possible correlations: Australian Geological Survey Organisation Journal of Australian Geology and Geophysics, v. 16, part 4, p. 587–608.

Gorter, J. D., 1998, The petroleum potential of Australian Phanerozoic impact structures: Australian Petroleum and Exploration Journal, v. 37, p. 159–186.

Green, D. H., 1981, Petrogenesis of Archaean ultramafic magmas and implications for Archaean tectonics, *in* Kroner, A., ed., Precambrian plate tectonics: Amsterdam, Elsevier, p. 469–489.

Grieve, R. A. F., 1980, Impact bombardment and its role in proto-continental growth of the early Earth: Precambrian Research, v. 10, p. 217–248.

Grieve, R. A. F., and Dence, M. R., 1979, The terrestrial cratering record: II. The crater production rate: Icarus, v. 38, p. 230–242.

Grieve, R. A. F., and Pesonen, L. J., 1996, Terrestrial impact craters: Their spatial and temporal distribution and impacting bodies: Earth, Moon, and Planets, v. 72, p. 357–376.

Grieve, R. A. F., and Pilkington, M., 1996, The signature of terrestrial impacts: Australian Geological Survey Organisation Journal of Australian Geology and Geophysics, v. 16, part 4, p. 399–420.

Grieve, R. A. F., and Shoemaker, E. M., 1994, The record of past impacts on Earth, *in* Gehrels, T., ed., Hazards due to comets and asteroids: Tucson, University of Arizona Press, p. 417–462.

Hart, R. J., Andreoli, M. A. G., Tredoux, M., Moser, D., Ashwal, L. D., Eide, E. A., Webb, S. J., and Brandt, D., 1997, Late Jurassic age for the Morokweng impact structure, southern Africa: Earth and Planetary Science Letters, v. 147, p. 25–35.

Hughs, H. G., App, F. N., and McGetchin, T. N., 1977, Global seismic effects of basin-forming impacts: Physics of the Earth and Planetary Interiors, v. 15, p. 251–263.

Jansa, L. F., 1993, Cometary impacts into ocean: Their recognition and the threshold constraints for biological extinction: Palaeogeography, Palaeoclimatology, Palaeoecology, v. 104, p. 271–286.

Jones, A. G., 1987, Are impact-generated lower crustal faults observable?: Earth and Planetary Science Letters, v. 85, p. 248–252.

McCulloch, M. T., and Bennett, V. C., 1994, Progressive growth of the Earth's continental crust and depleted mantle: Geochemical constraints: Geochimica et Cosmochimica Acta, v. 58, p. 4717–4738.

Moorbath, S., 1977, Ages, isotopes and evolution of the Precambrian crust: Chemical Geology, v. 20, p. 151–187.

Oberbeck, V. R., Marshall, J. R., and Aggarval, H., 1992, Impacts, tillites and the breakdown of Gondwanaland: Journal of Geology, v. 101, p. 1–19.

Pesonen, L. J., 1996, The impact cratering record of Fennoscandia: Earth, Moon, and Planets, v. 72, p. 377–393.

Roddy, D. J., Schuster, S. H., Rosenblatt, M., Grant, L. B., Hassig, P. J., and Kreyenhagen, K. N., 1987, Computer simulation of large asteroid impacts into oceanic and continental sites—Preliminary results on atmospheric, cratering and ejecta dynamics: International Journal of Impact Engineering, v. 5, p. 525–541.

Ryder, G., 1990, Lunar samples, lunar accretion and the early bombardment of the Moon: Eos (Transactions, American Geophysical Union), v. 71, p. 313–322.

Shoemaker, E. M., and Shoemaker, C. S., 1996, The Proterozoic impact record of Australia: Australian Geological Survey Organisation Journal of Australian Geology and Geophysics, v. 16, part 4, p. 379–398.

Manuscript received September 18, 1998
Revised manuscript received December 29, 1998
Manuscript accepted January 25, 1999